Multistable Kuramoto Splay States in a Crystal of Mode-Locked Laser Pulses

T. G. Seidel,[1,2] A. Bartolo,[3,4] A. Garnache,[3] M. Giudici,[4] M. Marconi,[4] S. V. Gurevich,[1,2] and J. Javaloyes[2]
[1]Institute for Theoretical Physics, University of Münster, Wilhelm-Klemm-Straße 9 48149 Münster, Germany
[2]Departament de Física and IAC[3], Universitat de les Illes Balears, C/ Valldemossa km 7.5, 07122 Mallorca, Spain
[3]Institut d'Electronique et des Systèmes, CNRS UMR5214, 34000 Montpellier, France
[4]Université Côte d'Azur, CNRS, Institut de Physique de Nice, 06200 Nice, France

(Received 11 March 2024; revised 19 July 2024; accepted 18 November 2024; published 22 January 2025)

We demonstrate the existence of coexisting frequency combs in a harmonically mode-locked laser that we link to the splay phases of the Kuramoto model with short range interactions. These splay states are multistable and the laser may wander between them under the influence of stochastic forces. Consequently, the many pulses circulating in the cavity are not necessarily coherent with each other. As these partially disordered states for the phase of the field still feature regular intensity pulses, we term them as incoherent crystals of optical pulses. We provide evidence that the notion of coherence should be interpreted by comparing the duration of the measurement time with the Kramers' escape time of each splay state. Our theoretical results are confirmed experimentally by performing high resolution spectral measurements via a heterodyne technique of a passively mode-locked vertical external-cavity surface-emitting laser.

DOI: 10.1103/PhysRevLett.134.033801

The realization of mode locking (ML) has been a milestone of laser physics as it allowed us to generate the ultrashort pulses that are of paramount importance in many fields [1]. The term ML stems from the synchronous oscillation, i.e., the phase locking of many electromagnetic modes in a cavity. The emergence of such macroscopic coherent states, either spontaneously or under periodic forcing, can be seen as the critical point of an equilibrium phase transition [2–4] establishing a link between modal self-organization and frequency combs in active cavities [5,6]. The applications of ML encompass radio-over-fiber [7], two-photon absorption microscopy [8] or dual comb spectroscopy [9]. The fundamental importance of mode-locked lasers is demonstrated by their link with dissipative solitons [10], their generalization to spatiotemporal systems [11–14] or their capability as Ising photonic machines to solve non-deterministic polynomial-time (NP) hard problems and perform Boltzmann sampling [15–17].

A pulsating laser can operate in the harmonic mode-locked (HML) regime, a state in which the laser cavity supports a train of $N \in \mathbb{N}$ equidistant pulses (denoted as HML_N) [18], see Fig. 1(a). This effectively reduces the pulse train period to τ/N with τ the cavity round trip, while circumventing the difficulties inherent in using shorter cavities. These regular pulse arrangements can be identified spectrally since the repetition rate multiplication corresponds to an equivalent N-fold increase in the distance between spectral lines that becomes a multiple of the fundamental free spectral range (FSR), i.e., N/τ. Such states have been widely observed in mode-locked fiber lasers [19–21] but also in optical systems with broken phase symmetry such as optically injected Kerr microcavities [22,23]. In the latter, regular pulse trains, also termed "soliton crystals," are phase locked to an external reference beam which leads to a unique, well-defined, frequency comb. The phase invariance of the field in a mode-locked laser radically modifies the picture as it allows each pulse to possess a *different* phase φ_i with $i \in [1, N]$, see Fig. 1(b).

In this Letter, we ask the seemingly naive question: are the N pulses circulating in a HML cavity necessarily coherent with each other? What are their phase relations (if any), and could an incoherent mode-locked crystal of pulses simply exist? To answer this question and, at variance with [2–4], we consider the phases of the pulses, instead of, those of the cavity modes, in a dissipative, out-from-equilibrium, framework.

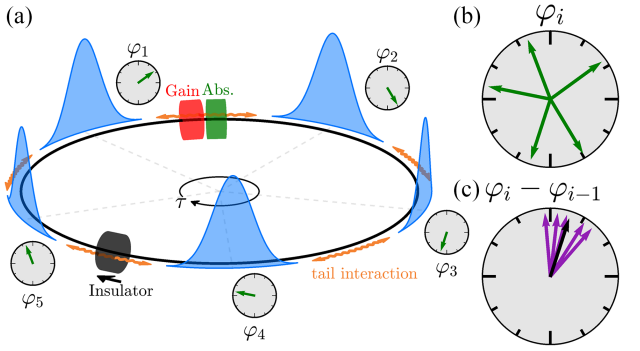

FIG. 1. (a) Schematic of a unidirectional ring cavity mode locked by a saturable absorber and operated in the HML_5 regime. Each pulse possesses a phase φ_i, as indicated by the small clocks. The phases and their differences are shown in (b) and (c) while the black arrow in (c) denotes the value of the order parameter b representing the average coherence.

We shall consider a passively mode-locked unidirectional ring laser as depicted in Fig. 1 in which a saturable absorber promotes pulsed emission. We study the HML dynamics using the well-established Haus master equation [24–26] that links the evolution of the electric field (E), the gain (g), and absorber population (q),

$$\partial_\theta E = \left(\frac{1}{2\gamma_f^2}\partial_z^2 + \frac{1-i\alpha_g}{2}g - \frac{1-i\alpha_q}{2}q - k\right)E + \sigma\xi, \quad (1)$$

$$\partial_z g = \Gamma(g_0 - g) - g|E|^2, \qquad \partial_z q = q_0 - q - sq|E|^2. \quad (2)$$

Here, z and θ denote the fast and slow timescales which describe the evolution within one round trip and from one round trip to the next one, respectively. Further, the gain bandwidth is γ_f, the cavity losses are k and $\alpha_{g,q}$ correspond either to the linewidth enhancement factors for semiconductor material or the transition line detuning in atomic gain media. Time is normalized to the absorber recovery time of 80 ps and the gain recovery rate is denoted as Γ, while the ratio of the saturation energy of the gain and the absorber media is s. For simplicity, we model the spontaneous emission fluctuations and the mechanical vibrations in the cavity potentially impacting coherence with a (normalized) white Gaussian stochastic process (ξ). The noise amplitude in Eq. (1) is σ. Equations (1) and (2) were complemented with the dynamical boundary conditions detailed in [26]. However, identical conclusions were obtained using periodic boundaries or by using a more refined model [27] and for widely different parameter values, see Supplemental Material (SM) [28]. The coherence of a regular HML state can be measured by *the order parameter* $b = (1/N)\sum_j \exp[i(\varphi_j - \varphi_{j-1})]$, which is equivalent to the first order field correlation $g^{(1)}(\tau/N)$ for a train of equidistant pulses that are identical up to a phase, see SM [28]. Perfect order corresponds to $|\langle b\rangle| = 1$, see Fig. 1(c), whereas full disorder yields $|\langle b\rangle| = 0$. The bracket denotes a temporal average over many cavity round trips. In order to derive in which configurations the pulses can exist in an HML regime, it is sufficient to consider the ring boundary conditions in Fig. 1(a). We assume that the phase difference $\Delta\varphi$ between neighboring pulses is constant, a condition fulfilled only for $N\Delta\varphi = 2\pi p$ with $p \in [0, N-1]$. We characterize the steady states by the integer index p or equivalently a phase difference $\Delta\varphi_p = (2\pi/N)p$. This is the definition of *a splay state* [29]. We note that a phase shift $\Delta\varphi_p$ between pulses separated by a distance $\Delta z = \tau/N$ corresponds to an offset of the carrier frequency $\nu_p = \Delta\varphi_p/(2\pi\Delta z) = p/\tau$. Consequently, these N splay states correspond to frequency combs that are shifted of p times the fundamental FSR of the cavity.

When a pulse crosses over the amplifier, it depletes its available gain, that only partially recovers before the arrival of the next pulse. This leads to a repulsion between pulses [30,31]. For short cavities where $\Gamma\tau < 1$, the positions of the pulses are tightly bound, as in a crystal, to $z_j = j\tau/N$. Pulses also possess phase sensitive interactions with their neighbors via the overlap of their decaying tails, see Fig. 1(a). Assuming exponential tails, this coherent effect scales as $\exp(-\tau_s/\tau_p) \ll 1$ with τ_s the separation between pulses and τ_p the pulse width. Consequently, the phase of each pulse evolves in relation with that of its nearest neighbors over a timescale much larger than the round trip. Notice that previous works demonstrated coherence in a HML laser with a ratio $\tau_s/\tau_p \simeq 23$ [20] indicating that this nearest neighbor interaction is extremely weak. While ratios up to $\tau_s/\tau_p \simeq 50$ were reported in [32], the impact of these interactions must be contrasted with the amount of spontaneous emission and technical noise destroying coherence.

The phase dynamics being the slowest variables, their evolution can be obtained by projecting the dynamics of the Eqs. (1) and (2) onto the central manifold, leading to

$$\partial_\theta\varphi_j = A_+\sin(\varphi_{j-1} - \varphi_j + \psi_+) + A_-\sin(\varphi_{j+1} - \varphi_j + \psi_-) + \xi_j, \qquad \varphi_0 = \varphi_N, j \in [1, N]. \quad (3)$$

We denote $(A_\pm, \psi_\pm)$ the amplitudes and phases of the coupling forces that originate from the overlap between the pulse and its nearest neighbors. Equation (3) captures the essence of the dynamics since $(A_\pm, \psi_\pm)$ depends effectively on all of the laser parameters. For $\psi_\pm \neq 0$ the interactions are nonvariational. In addition, since the pulses tails are *a priori* not symmetrical, $A_+ \neq A_-$ rendering interactions nonreciprocal [33,34]. Note that changing the parameters of the HML system will influence the phase dynamics only as much as it modifies $(A_\pm, \psi_\pm)$. Finally, ξ_j is a Gaussian white noise whose amplitude corresponds to the projection of the original stochastic process in Eq. (1) over the phase dynamics. Equations (3) correspond to the Kuramoto model with nearest neighbor interactions, also known as the dissipative XY model, see [35] and references therein. A linear stability analysis of Eq. (3) reveals that a splay state is stable if $\alpha_0 < \Delta\varphi_p < \alpha_1$ with α_k given by the following expression

$$\alpha_k = k\pi + \arctan\left(\frac{A_-\cos\psi_- + A_+\cos\psi_+}{A_-\sin\psi_- - A_+\sin\psi_+}\right). \quad (4)$$

We observe that the range of stability is always π and that the half-circle of stability is simply rotated as a function of

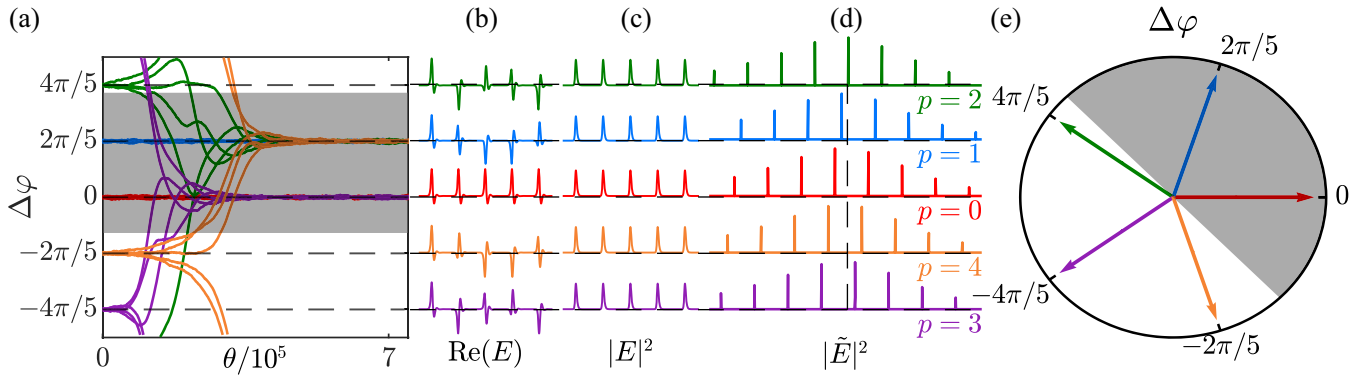

FIG. 2. (a) Evolution over the slow time θ of various splay states associated to the HML_5 solutions obtained from solving Eqs. (1) and (2) numerically. The initial phase differences are given by $\Delta\varphi_p = (2\pi/N)p$, and are shown in panels (b) and (c) where one can see that the intensity profiles are identical while the real parts of the electric fields differ. (d) Frequency spectrum of the initial conditions. For each phase difference the corresponding comb is shifted by (p/τ). (e) Phase plane visualization of the initial conditions used in (a)–(d). The shaded gray areas in panels (a) and (e) correspond to the region of stability which is of size π. The trajectories in (a) converge to steady states within the region of stability. Parameters are $(\gamma_f, k, \alpha_g, \alpha_q, \tau, g_0, \Gamma, q_0, s, \sigma) = (40, 0.1056, 1.5, 0.5, 12.5, 4g_{\mathrm{th}}, 0.08, 0.27, 10, 10^{-5})$ and correspond to a 5 GHz mode-locked laser emitting 14 ps pulses (FWHM). The lasing threshold is defined as $g_{\mathrm{th}} = q_0 + 2k$.

$(A_\pm, \psi_\pm)$. The most important consequence of Eq. (4) is that the splay states that are solutions of Eq. (3) can be *multistable*. In fact, for $N \geq 5$, there must be at least two states that fall within the range of stability and 50% of states are stable in the thermodynamic limit $N \to \infty$. In order to test our predictions we simulated numerically Eqs. (1) and (2), which we initialized with the five different splay states, see Figs. 2(a) and 2(b). All these solutions correspond to the same intensity profile as demonstrated in Fig. 2(c). The rotation of the field $\Delta\varphi_p$ from one pulse to the next creates a p/τ frequency-shifted comb, see Fig. 2(d). We observe that two initial conditions remain stable upon their time evolution as they lie within the stable region defined by Eq. (4) and marked by the gray areas in Figs. 2(a) and 2(e). The other three trajectories correspond to unstable states and converge to one of the two stable configurations, cf. Fig. 2(a). The parameters $(A_\pm, \psi_\pm)$ in Eq. (3) were extracted from Eqs. (1) and (2) by using a perturbation analysis around each splay state.

The prediction of multistability for $N \geq 5$ has a profound consequence on the measurement of the coherence as it must be interpreted by comparing the Kramers' escape time of each splay state [36] with the measurement time. The latter typically occurs experimentally over several tens of milliseconds, which corresponds to millions of round trips. We show in Fig. 3(a) the result of a long simulation of Eqs. (1) and (2) over 10^8 round trips, i.e., $\sim$0.4 s for $\tau = 4.4$ ns. Because of noise, the system is able to visit many times all the stable states. This is best observed in Fig. 3(b) which provides a close-up around a small part of the original time trace. Note that visiting the unstable states is also possible for higher noise amplitudes and that the noise amplitude used here only gives rise to a 5% fluctuation of the pulse peak power (cf. Figs. 2 and 3 of SM [28]). We detail in Fig. 3(c) a histogram of the value of arg b. Because of the low noise value, the distribution is narrowly peaked around each stable splay state and the theoretical value of the order parameter should be $\langle b_p \rangle = \exp(i\Delta\varphi_p)$. Indeed, if the value of the coherence $|\langle b \rangle|$ is calculated over a time smaller than the average residence time, we obtain $|\langle b \rangle| \sim 0.95$. If instead the coherence is measured over the entire time trace, $|\langle b \rangle| = 0.63$; this is the result of the partial cancellation between $\langle b_0 \rangle$ and $\langle b_1 \rangle$. Hence, in this system, the ergodic hypothesis that consists in replacing statistical (ensemble) average by a single realization of a stochastic process is valid only for extremely long measurement times. We envision this effect to become even more prominent for

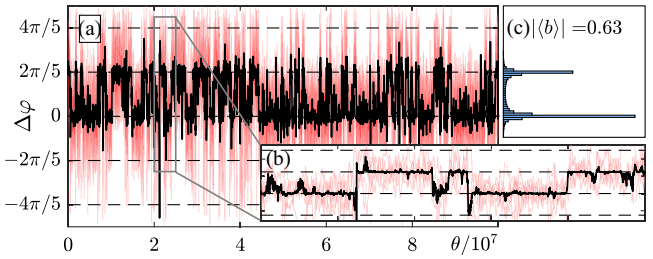

FIG. 3. (a) Time evolution over slow time θ of phase differences for five pulses (light red) for the same parameters as in Fig. 2 obtained from a direct numerical simulation of Eqs. (1) and (2) with added noise of amplitude $\sigma = 4 \times 10^{-4}$. The black line denotes the phase of the order parameter b. As the system is bistable for $N = 5$, the order parameter jumps between the two stable steady states $\Delta\varphi_{0,1} = 0, (2\pi/5)$. (b) Enlarged view around a region with multiple jumps. (c) Statistical distribution of the phases visited by arg b. The two peaks correspond to the two aforementioned steady states.

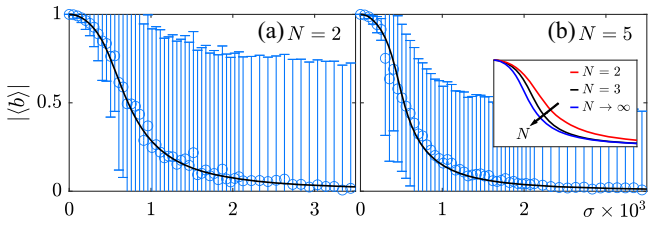

FIG. 4. The order parameter $|\langle b \rangle|$ as a function of noise for (a) $N = 2$ and (b) $N = 5$ pulses in the cavity [blue: Haus Eqs. (1) and (2), black: phase model in Eq. (3)]. The cavity round trip is increased according to the HML number as $\tau = N \times 2.5$. Same parameters as in Figs. 2 and 3. Inset in (b): analytical result for the Hamiltonian phase model.

higher number of pulses leading to a larger number of attractors in which the system may remain frozen.

Having demonstrated the good agreement between Eqs. (1) and (2) and Eq. (3), we performed an extended analysis as a function of N and the noise level using Eq. (3). Our results are summarized in Fig. 4. If the amplitude of the noise is too low, the system will not be able to jump from one steady state to the other leading to a coherence close to unity. If it is too high, i.e., $\sigma \gg A_{\pm}$, coherence is entirely lost as $|\langle b \rangle| \to 0$. Yet in this case the system continues to generate a very regular intensity pulse train and it can therefore be interpreted as an *incoherent crystal*. Finally, the coherence decays faster for larger values of N as it is averaged over a larger number of states. The numerical curves in Fig. 4 (in blue) were fitted with the analytical formula for the coherence (in black) of the Hamiltonian XY model [37] that shares the same steady states as Eq. (3) (cf. SM [28] for details).

To confirm our theoretical predictions, we implemented an experimental setup consisting of a vertical external-cavity surface-emitting laser (VECSEL) mode-locked using a semiconductor saturable absorber mirror as in [38]. The laser cavity (see SM [28]) has a round trip time $\tau = 8.5$ ns. For this value of τ, the optical pulses can be addressed on and off independently [39,40] although they become equidistant rapidly due to the repulsive incoherent forces discussed above. This leads to the multistability of the HML states with $N \in [0, 8]$. The laser output is sent to a heterodyne measurement setup that analyzes the spectral features of the pulse train. By beating the laser output with a stable CW laser source, we convert a portion of the optical spectrum into the radio-frequency (rf) domain (see SM [28]). We analyze the coherence of a pulse train consisting of four equidistant pulses. Figure 5(a) shows a spatiotemporal map of the laser intensity for the HML_4 solution, where the horizontal axis represents the round-trip time and the vertical axis is the number of round trips, which highlights that the pulses are perfectly equispaced, have the same amplitude, and are stable over more than 10^4 round trips. Figures 5(b) and 5(c) describe the principle of the heterodyne measurement. Panel (b) schematically illustrates the optical spectrum of a mode-locked laser that is emitting on a coherent splay state with $N = 4$. Because of the coherent interaction between the pulses, the spectrum is composed of equidistant lines every 4 FSR. The CW laser frequency is represented in red and the beating frequencies are shown in green. The corresponding rf signal is shown in panel (c).

The jump from one coherent splay state $\Delta\varphi_p$ to another $\Delta\varphi_q$ should manifest in the optical spectrum by a $(p - q)$-harmonic FSR shift while the interference pattern should keep the same visibility (see SM [28]). The heterodyne optical spectra (cf. the right column of Fig. 5) reveal the various splay states explored by the system. Figure 5(d) shows a situation identical to the example depicted in panel (c), which indicates that the pulsed solution is a coherent splay state. In panel (e), the rf spectrum shows the same features as panel (d) but the lines in the optical spectrum are

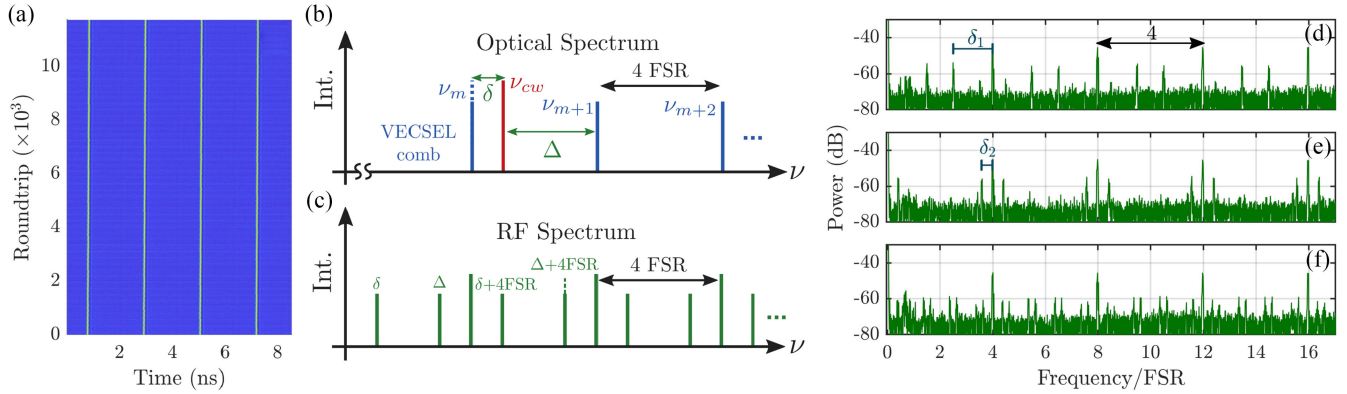

FIG. 5. (a) Space-time diagram of the laser output showing four equidistant pulses. (b) Schematic representation of an optical spectrum showing the CW laser line used for the heterodyne beating and the VECSEL comb for a splay state of four pulses. The frequency difference between the CW laser and the nearest comb line is δ. (c) Resulting heterodyne rf spectrum obtained from the signal in (b). (d), (e) Represent two heterodyne rf spectra showing a jump between two splay states spectrally separated by one FSR since $\delta_2 = \delta_1 - 1/\tau$. (f) rf spectrum of an incoherent state consisting of the average of all the splay states.

shifted with respect to the previous case. In accordance with the theory, the shift $|\delta_1 - \delta_2|$ experienced by the optical lines corresponds to one FSR of the laser optical spectrum, as demonstrated in SM [28]. Figure 5(f) reveals that the pulse train can also be incoherent, as predicted theoretically. This incoherent state is characterized by phase jumps which are responsible for the emergence of multiple beating lines in the optical spectrum. Here, the maximum number of 8 lines (2 beat tones times 4 possible FSR jumps) is obtained, indicating that within the acquisition time of the rf spectrum analyzer (20 ms), the phase differences between pulses have explored all the four stable and unstable possible configurations (from 0 to $3\pi/4$). This demonstrates that a pulse train can be stable in intensity, while the phase difference between consecutive pulses can vary in time. Similar results were obtained for a larger number of pulses, see SM [28], and different current values.

In conclusion, we demonstrated that the harmonic pulse trains emitted by a mode-locked laser are equivalent to the splay-phase states of the Kuramoto model with short range interactions. The multistability between frequency combs was experimentally observed. The evolution of the coherence between high and small values confirms that this notion must be interpreted by comparing the duration of the measurement time with the Kramers' escape time of each splay state. These partially disordered states for the phase feature regular intensity pulse trains which we term incoherent optical crystals. Our minimal model was sufficient to explain the experiment. However, additional couplings arising from time-delayed feedback, as in [40], or intracavity lenses reflection would induce further nonlocal coupling between pulses and lead to an even richer phenomenology, as observed in other fields [41–43].

Acknowledgments—We acknowledge the financial support of the project KOGIT, Agence Nationale de la Recherche (No. ANR-22-CE92-0009) and Deutsche Forschungsgemeinschaft (DFG) via Grant No. 505936983. T. G. S. and J. J. acknowledge funding from the Studienstiftung des Deutschen Volkes and the KEFIR/AEI/10.13039/501100011033/FEDER, UE, respectively.

[1] H. A. Haus, Mode-locking of lasers, IEEE J. Selected Topics Quantum Electron. **6**, 1173 (2000).
[2] A. Gordon and B. Fischer, Phase transition theory of many-mode ordering and pulse formation in lasers, Phys. Rev. Lett. **89**, 103901 (2002).
[3] R. Weill, A. Rosen, A. Gordon, O. Gat, and B. Fischer, Critical behavior of light in mode-locked lasers, Phys. Rev. Lett. **95**, 013903 (2005).
[4] L. Leuzzi, C. Conti, V. Folli, L. Angelani, and G. Ruocco, Phase diagram and complexity of mode-locked lasers: From order to disorder, Phys. Rev. Lett. **102**, 083901 (2009).
[5] Johannes Hillbrand, Dominik Auth, Marco Piccardo, Nikola Opačak, Erich Gornik, Gottfried Strasser, Federico Capasso, Stefan Breuer, and Benedikt Schwarz, In-phase and anti-phase synchronization in a laser frequency comb, Phys. Rev. Lett. **124**, 023901 (2020).
[6] L. Columbo, M. Piccardo, F. Prati, L. A. Lugiato, M. Brambilla, A. Gatti, C. Silvestri, M. Gioannini, N. Opačak, B. Schwarz, and F. Capasso, Unifying frequency combs in active and passive cavities: Temporal solitons in externally driven ring lasers, Phys. Rev. Lett. **126**, 173903 (2021).
[7] D. Novak, Z. Ahmed, R. B. Waterhouse, and R. S. Tucker, Signal generation using pulsed semiconductor lasers for application in millimeter-wave wireless links, IEEE Trans. Microwave Theory Techn. **43**, 2257 (1995).
[8] Masaru Kuramoto, Nobuyoshi Kitajima, Hengchang Guo, Yuji Furushima, Masao Ikeda, and Hiroyuki Yokoyama, Two-photon fluorescence bioimaging with an all-semiconductor laser picosecond pulse source, Opt. Lett. **32**, 2726 (2007).
[9] S. M. Link, D. J. H. C. Maas, D. Waldburger, and U. Keller, Dual-comb spectroscopy of water vapor with a free-running semiconductor disk laser, Science **356**, 1164 (2017).
[10] P. Grelu and N. Akhmediev, Dissipative solitons for mode-locked lasers, Nat. Photonics **6**, 84 (2012).
[11] Aleksander K. Wójcik, Nanfang Yu, Laurent Diehl, Federico Capasso, and Alexey Belyanin, Self-synchronization of laser modes and multistability in quantum cascade lasers, Phys. Rev. Lett. **106**, 133902 (2011).
[12] Logan G. Wright, Pavel Sidorenko, Hamed Pourbeyram, Zachary M. Ziegler, Andrei Isichenko, Boris A. Malomed, Curtis R. Menyuk, Demetrios N. Christodoulides, and Frank W. Wise, Mechanisms of spatiotemporal mode-locking, Nat. Phys. **16**, 565 (2020).
[13] Yihang Ding, Xiaosheng Xiao, Kewei Liu, Shuzheng Fan, Xiaoguang Zhang, and Changxi Yang, Spatiotemporal mode-locking in lasers with large modal dispersion, Phys. Rev. Lett. **126**, 093901 (2021).
[14] Logan G. Wright, William H. Renninger, Demetri N. Christodoulides, and Frank W. Wise, Nonlinear multimode photonics: Nonlinear optics with many degrees of freedom, Optica **9**, 824 (2022).
[15] Shuhei Tamate, Yoshihisa Yamamoto, Alireza Marandi, Peter McMahon, and Shoko Utsunomiya, Simulating the classical XY model with a laser network, arXiv:1608.00358.
[16] Takahiro Inagaki, Kensuke Inaba, Ryan Hamerly, Kyo Inoue, Yoshihisa Yamamoto, and Hiroki Takesue, Large-scale Ising spin network based on degenerate optical parametric oscillators, Nat. Photonics **10**, 415 (2016).
[17] Y. Takeda, S. Tamate, Y. Yamamoto, H. Takesue, T. Inagaki, and S. Utsunomiya, Boltzmann sampling for an *XY* model using a non-degenerate optical parametric oscillator network, Quantum Sci. Technol. **3**, 014004 (2017).
[18] M. Becker, D. Kuizenga, and A. Siegman, Harmonic mode locking of the Nd:YAG laser, IEEE J. Quantum Electron. **8**, 687 (1972).
[19] A. B. Grudinin and S. Gray, Passive harmonic mode locking in soliton fiber lasers, J. Opt. Soc. Am. B **14**, 144 (1997).
[20] Adil Haboucha, Hervé Leblond, Mohamed Salhi, Andrey Komarov, and François Sanchez, Coherent soliton pattern formation in a fiber laser, Opt. Lett. **33**, 524 (2008).

[21] Foued Amrani, Mohamed Salhi, Philippe Grelu, Hervé Leblond, and François Sanchez, Universal soliton pattern formations in passively mode-locked fiber lasers, Opt. Lett. **36**, 1545 (2011).
[22] Daniel C. Cole, Erin S. Lamb, Pascal Del'Haye, Scott A. Diddams, and Scott B. Papp, Soliton crystals in Kerr resonators, Nat. Photonics **11**, 671 (2017).
[23] Maxim Karpov, Martin H. P. Pfeiffer, Hairun Guo, Wenle Weng, Junqiu Liu, and Tobias J. Kippenberg, Dynamics of soliton crystals in optical microresonators, Nat. Phys. **15**, 1071 (2019).
[24] H. A. Haus, M. Margalit, and C. X. Yu, Quantum noise of a mode-locked laser, J. Opt. Soc. Am. B **17**, 1240 (2000).
[25] A. M. Perego, B. Garbin, F. Gustave, S. Barland, F. Prati, and G. J. de Valcárcel, Coherent master equation for laser modelocking, Nat. Commun. **11**, 311 (2020).
[26] Jan Hausen, Kathy Lüdge, Svetlana V. Gurevich, and Julien Javaloyes, How carrier memory enters the Haus master equation of mode-locking, Opt. Lett. **45**, 6210 (2020).
[27] A. G. Vladimirov and D. Turaev, Model for passive mode locking in semiconductor lasers, Phys. Rev. A **72**, 033808 (2005).
[28] See Supplemental Material at http://link.aps.org/supplemental/10.1103/PhysRevLett.134.033801 for theoretical background of the order parameter; presentation of analogue results in a time-delayed model; experimental setup; explanation of the beat heterodyne spectrum.
[29] Rico Berner, Serhiy Yanchuk, Yuri Maistrenko, and Eckehard Schöll, Generalized splay states in phase oscillator networks, Chaos **31**, 073128 (2021).
[30] J. N. Kutz, B. C. Collings, K. Bergman, and W. H. Knox, Stabilized pulse spacing in soliton lasers due to gain depletion and recovery, IEEE J. Quantum Electron. **34**, 1749 (1998).
[31] J. Javaloyes, P. Camelin, M. Marconi, and M. Giudici, Dynamics of localized structures in systems with broken parity symmetry, Phys. Rev. Lett. **116**, 133901 (2016).
[32] Philippe Grelu, Franck Belhache, François Gutty, and Jose M. Soto-Crespo, Relative phase locking of pulses in a passively mode-locked fiber laser, J. Opt. Soc. Am. B **20**, 863 (2003).
[33] Michel Fruchart, Ryo Hanai, Peter B. Littlewood, and Vincenzo Vitelli, Non-reciprocal phase transitions, Nature (London) **592**, 363 (2021).
[34] Sabine H. L. Klapp, Non-reciprocal interaction for living matter, Nat. Nanotechnol. **18**, 8 (2023).
[35] Juan A. Acebrón, L. L. Bonilla, Conrad J. Pérez Vicente, Félix Ritort, and Renato Spigler, The Kuramoto model: A simple paradigm for synchronization phenomena, Rev. Mod. Phys. **77**, 137 (2005).
[36] C. W. Gardiner, *Handbook of Stochastic Methods*, 2nd ed. (Springer-Verlag, Berlin, 1995).
[37] J. M. Kosterlitz and D. J. Thouless, Ordering, metastability and phase transitions in two-dimensional systems, J. Phys. C **6**, 1181 (1973).
[38] A. Bartolo, N. Vigne, M. Marconi, G. Beaudoin, K. Pantzas, I. Sagnes, G. Huyet, F. Maucher, S. V. Gurevich, J. Javaloyes, A. Garnache, and M. Giudici, Temporal localized turing patterns in mode-locked semiconductor lasers, Optica **9**, 1386 (2022).
[39] P. Camelin, C. Schelte, A. Verschelde, A. Garnache, G. Beaudoin, I. Sagnes, G. Huyet, J. Javaloyes, S. V. Gurevich, and M. Giudici, Temporal localized structures in mode-locked vertical external-cavity surface-emitting lasers, Opt. Lett. **43**, 5367 (2018).
[40] A. Bartolo, T. G. Seidel, N. Vigne, A. Garnache, G. Beaudoin, I. Sagnes, M. Giudici, J. Javaloyes, S. V. Gurevich, and M. Marconi, Manipulation of temporal localized structures in a vertical external-cavity surface-emitting laser with optical feedback, Opt. Lett. **46**, 1109 (2021).
[41] M. A. Fuentes, M. N. Kuperman, and V. M. Kenkre, Nonlocal interaction effects on pattern formation in population dynamics, Phys. Rev. Lett. **91**, 158104 (2003).
[42] F. Maucher, T. Pohl, S. Skupin, and W. Krolikowski, Self-organization of light in optical media with competing nonlinearities, Phys. Rev. Lett. **116**, 163902 (2016).
[43] J. Javaloyes, M. Marconi, and M. Giudici, Nonlocality induces chains of nested dissipative solitons, Phys. Rev. Lett. **119**, 033904 (2017).